J. Min. Metall. Sect. B-Metall. 53 (3) B (2017) 179 - 187

Journal of Mining and Metallurgy, Section B: Metallurgy

THERMODYNAMIC ASSESSMENT OF THE Pb–Sr SYSTEM

H. Zhang [a], C. Zhang [b], W.W. Wang [c], Y. Du [a,*], P. Zhou [d], B. Hu [e], Z. Liu [a], J.C. Wang [a], J. Wang [a]

[a] State Key Laboratory of Powder Metallurgy, Central South University, Changsha, Hunan, PR China
[b] Collaborative Innovation Center of Steel Technology, University of Science and Technology Beijing, Beijing, PR China
[c] Company of Hunan Liugu Grand Pharmacy, Hunan, PR China
[d] College of Mechanical and Electrical Engineering, Hunan University of Science and Technology, Xiangtan, PR China
[e] School of Materials Science and Engineering, Anhui University of Science and Technology, Huainan, PR China

(Received 02 March 2017; accepted 25 July 2017)

Abstract

The Pb-Sr system has been critically reviewed and modeled by means of the CALPHAD (CALculation of PHAse Diagrams) approach. It contains seven stoichiometric compounds, i.e. $SrPb_3$, Sr_3Pb_5, Sr_2Pb_3, SrPb, Sr_5Pb_4, Sr_5Pb_3 and Sr_2Pb, in which the $SrPb_3$ and Sr_2Pb phases melt congruently, and the other five phases form via peritectic reactions. The enthalpies of formation for the intermetallic compounds at 0 K are provided by first-principles calculations. The liquid, fcc and bcc phases are modeled as substitutional solution phases. Both Redlich-Kister and exponential polynomials are used to describe the excess Gibbs energy of the liquid. Two sets of self-consistent thermodynamic parameters are obtained by considering reliable experimental data and the computed enthalpies of formation. Comprehensive comparisons between the calculated and measured phase diagram and thermodynamic data show that the experimental information is satisfactorily accounted for by the present thermodynamic description.

Keywords: *Pb–Sr system; Thermodynamics; Phase diagram; First-principles calculations.*

1. Introduction

Knowledge of the physical properties in Pb-based alloys is of great importance in industrial applications such as grid material and lead-acid batteries. One of important Pb-based binary alloy systems is the Ca–Pb system, which is widely used in the maintenance-free lead-acid batteries, as it can improve storage life and reduce self-discharge. The disadvantages are its poor strength, casting difficulties and low resistance to discharge cycle capacity [1, 2]. The Pb–Sr alloy can satisfy the maintenance of free performance and realize deep cycle discharge performance as well as corrosion resistance requirements [3, 4].

There have been several experimental determinations on the phase equilibria of the Pb–Sr system [5–8]. The comprehensive determinations by Bruzzone et al. [6] were redrawn by Massalski [9]. However, there is no general agreement between the proposed phase diagram and thermodynamic data. The present work is thus devoted to the assessment of experimental phase diagram and thermodynamic data available for the Pb–Sr system via the CALPHAD approach, which is a common method in the thermodynamic field and has been used for many systems [10–12], and provide two optimal sets of thermodynamic parameters for this system by using both Redlich-Kister linear [13] and exponential polynomials [14].

2. Literature review

2.1 Phase diagram data

In the present assessment, the reported experimental phase diagram and thermodynamic data of the Pb–Sr system were critically reviewed. The experimental phase diagram data have been measured by four groups of authors [5–8]. Seven intermetallic compounds, i.e. $SrPb_3$, Sr_3Pb_5, Sr_2Pb_3, SrPb, Sr_5Pb_4, Sr_5Pb_3 and Sr_2Pb, were identified to be stable in this system.

Using differential thermal analysis (DTA), X-ray diffraction (XRD), chemical analysis (CA), microhardness measurement (MHM), spectrophotometric analysis (SA) and optical metallography (OM), Vakhobov et al. [5] studied the phase equilibria of Pb–Sr system. In

Dedicated to the memory of Professor Dragana Živković

* *Corresponding author: yong-du@csu.edu.cn*

DOI:10.2298/JMMB170302013Z

the composition range of 0 at.% to 25 at.% Sr, a mixture of primary $SrPb_3$ crystals and β (the solid solution of Sr in Pb) eutectic was formed. At 900 °C, there is a peritectic reaction, L + Sr_2Pb ↔ SrPb. The congruent melting of Sr_2Pb compound with a melting point of 970 °C was observed [5], while the melting point for Sr_2Pb is 1155 °C according to Bruzzone et al. [6]. The experimental results given by Vakhobov et al. [5] are different from those of Bruzzone et al. [6] and Marshall and Chang [7]. Moreover, only the L + Sr_2Pb ↔ SrPb peritectic reaction was detected by Vakhobov et al. [5], and the other four peritectic reactions were not determined. The temperature is 630 °C for the eutectic reaction in the Sr-rich part of the system [5]. However, the temperature for the above eutectic reaction is 725 °C according to Bruzzone et al. [6]. Since the method for the preparation of Pb–Sr alloys by Vakhobov et al. [5] could lead to the melting of Pb and Sr in corundum crucibles, in which the specimens were obtained by combining the processes of vacuum distillation and directional solidification, this processes cannot ensure the homogeneous specimens. Therefore, the data published by Vakhobov et al. [5] were not used in the present optimization.

The Pb–Sr system was investigated by Bruzzone et al. [6] using OM, XRD and thermal analysis (TA). Seven intermediate phases were found by them [6]. Two of these phases melt congruently: Sr_2Pb (1155 °C) and $SrPb_3$ (675 °C). The remaining five phases form peritectically: Sr_5Pb_3 (1054 °C), Sr_5Pb_4 (943 °C), SrPb (785 °C), Sr_2Pb_3 (717 °C) and Sr_3Pb_5 (645 °C). Two eutectic points were found to be at 87.5 at.% Sr (725 °C) and 30.5 at.% Sr (627 °C), respectively. The crystal structure data of the compounds Sr_2Pb (anti-$PbCl_2$ type), Sr_5Pb_3 (Cr_5B_3 type), SrPb (CrB type) and $SrPb_3$ (Ti_3Cu type) were also provided [6]. The lattice parameters and prototypes of Sr_5Pb_4, Sr_2Pb_3 and Sr_3Pb_5 compounds were reported [6]. The detailed information [6, 15–23] on crystal structure data is summarized in Table 1.

Marshall and Chang [7] studied the phase equilibria of the Pb–Sr system in the composition range up to 36 at.% Sr by using DTA, OM, XRD and electron probe micro analysis (EPMA). An eutectic at 324.5 °C and 1.0 at.% Sr is formed between (Pb) and $SrPb_3$. According to DTA results [7], the maximum Sr content in the lead solid solution is approximate 0.33 at.%. $SrPb_3$ was found to melt congruently at 677 °C, which is in good agreement with the values 676 °C [8] and 675 °C [6]. The liquidus from 0 to 25 at.% Sr [7] is consistent with those given by Piwowarsky [8] and Bruzzone et al. [6]. Those experimental data are used in the present thermodynamic modeling.

2.2 Thermodynamic data

Using the first-principles method, Duan et al. [24] and Peng et al. [25] calculated the enthalpies of formation for the intermetallic compounds. The calculated enthalpies of formation for Sr_2Pb are –63.56 kJ/(mol·atom) at 0 K and 0 Gpa and –42.98 kJ/(mol·atom) at 0 K and 10 Gpa by Duan et al. [24]. The data by Duan et al. [24] are used in this work. The enthalpies of formation for the seven intermetallic compounds have been calculated by Peng et al. [25]. The enthalpy of formation for Sr_2Pb at 0 K is –61.951 kJ/(mol·atom) according to Peng et al. [25], which is more positive than the results by Duan et al. [24]. In this work, the enthalpies of formation for $SrPb_3$, Sr_2Pb_3, SrPb, Sr_5Pb_4, Sr_5Pb_3 and Sr_2Pb were also calculated and the detail will be discussed in Section 4.

The phase diagram and thermodynamic data of the Pb–Sr binary system evaluated above are summarized

Table 1. *Phase designation and crystal structure data for the solid phases in the Pb–Sr system.*

Phase	Prototype / Space group	Lattice parameters (Å)			Ref.
		a	b	c	
Sr_2Pb	Anti-$PbCl_2$ / Pnma	8.445	5.391	10.139	[15]
Sr_5Pb_3	Cr_5B_3 / I4/mcm	8.67	8.67	15.94	[16]
Sr_5Pb_4	Gd_5Si_4 / Pnma	8.48	17.21	9.01	[6]
SrPb	CrB / Cmcm	5.018	12.23	4.648	[17]
Sr_2Pb_3	Sr_2Pb_3	8.38	8.38	4.9	[6]
	Sr_2Pb_3 / P4/mbm	8.367	8.367	4.883	[18]
Sr_3Pb_5	Sr_3Pb_5	16.18	16.18	4.9	[6]
	Sr_3Pb_5 / P4/mbm	16.17	16.17	4.886	[18]
$SrPb_3$	Ti_3Cu	4.965	4.965	5.035	[19]
	$SrPb_3$ / P4/mmm	4.966	4.966	5.025	[20]
(Pb)	Cu / Fm-3m	4.95	4.95	4.95	[21]
(Sr)rt	Cu / Fm-3m	6.082	6.082	6.082	[22]
(Sr)ht	W / Im-3m	4.85	4.85	4.85	[23]

in Table 2, together with the indications whether the experimental data were used or not in this optimization.

Table 2. *Summary of the reported experimental data for the Pb–Sr system.*

Type of data	Ref.	Method [a]	Quoted mode [b]
Liquidus	[5]	DTA, XRD, OM, CA, MHM, SA	□
Eutectic temperature			
Peritectic temperature			
Congruent melting point			
Liquidus	[6]	TA, XRD, OM	■
Eutectic temperature			
Peritectic temperature			
Congruent melting point			
Crystal structures			
Liquidus (0-36 at.% Sr)	[7]	DTA, OM, EPMA, XRD	■
Solubility (Sr in Pb)			
Eutectic temperature			
Congruent melting point			
Liquidus (0-25 at.% Sr)	[8]	TA, OM	■
Congruent melting point			
Enthalpies of formation for compounds (Sr_2Pb)	[24]	First-Principles method	■
Enthalpies of formation for compounds ($SrPb_3$, Sr_3Pb_5, Sr_2Pb_3, SrPb, Sr_5Pb_4, Sr_5Pb_3, Sr_2Pb)	[25]	First-Principles method	■
Enthalpies of formation for compounds ($SrPb_3$, Sr_2Pb_3, SrPb, Sr_5Pb_4, Sr_5Pb_3, Sr_2Pb)	This work	First-Principles method	■

[a] For the experimental techniques: DTA = Differential thermal analysis; XRD = X-ray diffraction; OM = Optical metallography; CA = Chemical analysis; MHM = Microhardness measurement; SA = Spectrophotometric analysis; TA = Thermal analysis and EPMA = Electron probe micro analysis. [b] Indicates whether the data were used or not in the optimization process: ■ used; □ not used.

3. Thermodynamic modeling

3.1. Unary phases

The Gibbs energy function $G_i^{\varphi}(T) = {}^0G_i^{\varphi} - H_i^{SER}$ (298.15 K) for the element i (i = Pb, Sr) in the phase φ (φ = liquid, bcc_A2 and fcc_A1) is described by an equation of the form:

$$G_i^{\varphi}(T) = a + bT + cT\ln T + dT^2 + eT^3 + fT^{-1} + gT^7 + hT^{-9} \quad (1)$$

where H_i^{SER} (298.15 K) is the molar enthalpy of the element i at 298.15 K in its standard element reference (SER) states. In this work, the Gibbs energy functions are taken from the SGTE compilation by Dinsdale [26].

3.2. Solution phases

The liquid, fcc and bcc phases are described by a substitution solution model, and their molar Gibbs energies are given by the following formula:

$$G_m^{\varphi} = {}^{ref}G_m^{\varphi} + {}^{id}G_m^{\varphi} + {}^{ex}G_m^{\varphi} \quad (2)$$

in which ${}^{ref}G_m^{\varphi}$ is the contribution to the Gibbs energy from pure components, ${}^{id}G_m^{\varphi}$ is the ideal mixing contribution to Gibbs energy , and ${}^{ex}G_m^{\varphi}$ is the excess Gibbs energy corresponding to the non-ideal interactions between the components.

For the Pb-Sr system, the following equations hold:

$${}^{ref}G_m^{\phi}(T) = x_{Pb}\,{}^0G_{Pb}^{\phi}(T) + x_{Sr}\,{}^0G_{Sr}^{\phi}(T) \quad (3)$$

$${}^{id}G_m^{\varphi}(T) = RT(x_{Pb}\ln x_{Pb} + x_{Sr}\ln x_{Sr}) \quad (4)$$

where R is the gas constant, T is temperature in K, and x_{Pb} and x_{Sr} are the mole fractions of Pb and Sr, respectively.

The excess terms of the solution phases were modeled by the Redlich-Kister linear polynomial [13]. To avoid the artificial miscibility gap at high temperatures, the exponential equation [14] was also used for the excess Gibbs energy of the liquid phase.

$${}^{ex}G_m^{\varphi}(T) = x_{Pb}x_{Sr}\sum_{i=0}^{n} {}^iL_{Pb,Sr}^{\varphi}(T)(x_{Pb} - x_{Sr})^i \quad (5)$$

in which the interaction parameters are described as follows:

$${}^iL_{Pb,Sr}^{\varphi}(T) = a_i + b_iT \quad (6)$$

or,

$${}^iL_{Pb,Sr}^{\varphi}(T) = h_i\exp(-T/\tau_i) \quad (7)$$

where ${}^iL_{Pb,Sr}^{\varphi}(T)$ is the ith interaction parameter between the elements Pb and Sr. The coefficients a_i, h_i are the enthalpy part of the interaction energy, b_i is the entropy part of the interaction energy and τ_i (τ_i >0) is a special temperature. These parameters are to be optimized in the present work.

3.3. Stoichiometric compounds

In view of the negligible solubilities, all the intermetallic phases in the Pb–Sr system were modeled as stoichiometric compounds. The Gibbs energy of the stoichiometric compound ${}^0G^{Sr_mPb_n}$ is expressed as follows:

$${}^0G^{Sr_mPb_n} = m\,{}^0G_{Sr} + n\,{}^0G_{Pb} + A + BT \quad (8)$$

in which ${}^0G_{Sr}$ and ${}^0G_{Pb}$ are the Gibbs energies of the Sr and Pb pure elements, respectively. And A and B are the parameters to be evaluated.

4. Results and discussion

The evaluation of model parameters in the Pb–Sr binary system has been carried out by recurrent runs of the PARROT module in Thermo-Calc software [27], which works by minimizing the square sum of the differences between measured and calculated values. The step-by-step optimization procedure described by Du et al. [28] was utilized in the present assessment. Each piece of selected information was given a certain weight based on the uncertainties of the experimental data, and changed by trial and error during the assessment, until most of the selected experimental information was reproduced within the expected uncertainty limits.

In the present work, two methods were used to avoid the formation of an undesired miscibility gap in the liquid phase for the Pb–Sr phase diagram. Using the linear equation for the excess Gibbs energy of the liquid, constraints must be imposed during the optimization procedure [29, 30]. A positive curvature of the liquidus by restricting $d^2G/dx^2 > 0$ in the atomic composition range $0 \le x(Sr) \le 1$ was applied in the thermodynamic optimization. Another method is to apply the exponential equation [14] directly to describe the excess Gibbs energy of the liquid. The advantage of the exponential equation is that no constraint is needed during the thermodynamic optimization for the sake of avoiding the undesired miscibility gap in the liquid phase.

The optimization started with the liquid phase, and a thermodynamic parameter ${}^0L^{liquid}_{Pb,Sr}$ was adjusted based on the liquidus data [6–8]. Then the intermetallic compounds were taken into consideration. The enthalpies of formation for all intermetallic phases via first-principles calculations were used as initial values for the parameters *A* in Eq. (8) and the initial values of *B* obtained at random. After that, all the coefficients in Eq. (8) were optimized according to the phase diagram data [6–8]. At the same time, the parameters ${}^1L^{liquid}_{Pb,Sr}$ and ${}^2L^{liquid}_{Pb,Sr}$ were adjusted in order to have a good agreement between calculation and experiment. The optimized parameters for the liquid and compounds were then fixed during the next optimization procedure. Both (Pb) and (Sr)rt have fcc_A1 structure, in order to make the thermodynamic property of (Pb) independent from that of (Sr)rt, the parameters ${}^0L^{fcc}_{Pb,Sr:Va}$ and ${}^1L^{fcc}_{Pb,Sr:Va}$ for the fcc phase were optimized subsequently. Finally, all parameters for the individual phases were optimized simultaneously to achieve a global self-consistent thermodynamic description.

The presently obtained thermodynamic parameters for the Pb–Sr system are given in Table 3. Using these two sets of parameters, the phase equilibria, enthalpies of mixing for the liquid as well as the enthalpies of formation for the intermetallic phases in the Pb–Sr system are calculated to show the rationality of the present modeling.

Table 3. *Summary of the optimized thermodynamic parameters in the Pb–Sr system*

Phase	Type	Parameter [a]
Liquid: $(Pb, Sr)_1$	R-K linear model	${}^0L^{liquid}_{Pb,Sr} = -149772.0 - 25.53T$
		${}^1L^{liquid}_{Pb,Sr} = -31474.8 + 32.62T$
		${}^2L^{liquid}_{Pb,Sr} = +61064.7 - 16.44T$
	Exponential model	${}^0L^{liquid}_{Pb,Sr} = -156179.4\ \exp(-1.44\times10^{-7}\mathrm{T})$
		${}^1L^{liquid}_{Pb,Sr} = -144831.5\ \exp(-3.58\times10^{-3}\mathrm{T})$
		${}^2L^{liquid}_{Pb,Sr} = +84944.8\ \exp(-7.45\times10^{-4}\mathrm{T})$
fcc: $(Pb, Sr)_1$: $(Va)_1$	R-K linear model	${}^0L^{fcc}_{Pb,Sr:Va} = -120000$
		${}^1L^{fcc}_{Pb,Sr:Va} = 0$
	Exponential model	${}^0L^{fcc}_{Pb,Sr:Va} = -105000$
		${}^1L^{fcc}_{Pb,Sr:Va} = -9000$
$SrPb_3$: $(Pb)_{3/4}$: $(Sr)_{1/4}$	R-K linear model	$G^{SrPb_3}_{Pb:Sr} = 3/4\,{}^0G^{fcc}_{Pb} + 1/4\,{}^0G^{fcc}_{Sr} - 37044.8 + 0.15T$
	Exponential model	$G^{SrPb_3}_{Pb:Sr} = 3/4\,{}^0G^{fcc}_{Pb} + 1/4\,{}^0G^{fcc}_{Sr} - 37947.9+4.03\mathrm{T}$
Sr_3Pb_5: $(Pb)_{5/8}$: $(Sr)_{3/8}$	R-K linear model	$G^{Sr_3Pb_5}_{Pb:Sr} = 5/8\,{}^0G^{fcc}_{Pb} + 3/8\,{}^0G^{fcc}_{Sr} - 47373.1 + 0.45T$
	Exponential model	$G^{Sr_3Pb_5}_{Pb:Sr} = 5/8\,{}^0G^{fcc}_{Pb} + 3/8\,{}^0G^{fcc}_{Sr} - 47327.8+4.50\mathrm{T}$
Sr_2Pb_3: $(Pb)_{3/5}$: $(Sr)_{2/5}$	R-K linear model	$G^{Sr_2Pb_3}_{Pb:Sr} = 3/5\,{}^0G^{fcc}_{Pb} + 2/5\,{}^0G^{fcc}_{Sr} - 49494.8 + 0.71T$
	Exponential model	$G^{Sr_2Pb_3}_{Pb:Sr} = 3/5\,{}^0G^{fcc}_{Pb} + 2/5\,{}^0G^{fcc}_{Sr} - 49000+4.47\mathrm{T}$

Table 3 is continued on the next page.

Table 3 continues from the previous page

SrPb: $(Pb)_{1/2}$: $(Sr)_{1/2}$	R-K linear model	$G_{Pb:Sr}^{SrPb} = 1/2\,{}^0G_{Pb}^{fcc} + 1/2\,{}^0G_{Sr}^{fcc} - 53741.0 + 0.16T$
	Exponential model	$G_{Pb:Sr}^{SrPb} = 1/2\,{}^0G_{Pb}^{fcc} + 1/2\,{}^0G_{Sr}^{fcc} - 52359.4 + 4.06\mathrm{T}$
Sr_5Pb_4: $(Pb)_{4/9}$: $(Sr)_{5/9}$	R-K linear model	$G_{Pb:Sr}^{Sr_5Pb_4} = 4/9\,{}^0G_{Pb}^{fcc} + 5/9\,{}^0G_{Sr}^{fcc} - 56395.7 + 0.94T$
	Exponential model	$G_{Pb:Sr}^{Sr_5Pb_4} = 4/9\,{}^0G_{Pb}^{fcc} + 5/9\,{}^0G_{Sr}^{fcc} - 53804.9 + 4.17\mathrm{T}$
Sr_5Pb_3: $(Pb)_{3/8}$: $(Sr)_{5/8}$	R-K linear model	$G_{Pb:Sr}^{Sr_5Pb_3} = 3/8\,{}^0G_{Pb}^{fcc} + 5/8\,{}^0G_{Sr}^{fcc} - 56282.3 + 1.01T$
	Exponential model	$G_{Pb:Sr}^{Sr_5Pb_3} = 3/8\,{}^0G_{Pb}^{fcc} + 5/8\,{}^0G_{Sr}^{fcc} - 52591.7 + 3.72\mathrm{T}$
Sr_2Pb: $(Pb)_{1/3}$: $(Sr)_{2/3}$	R-K linear model	$G_{Pb:Sr}^{Sr_2Pb} = 1/3\,{}^0G_{Pb}^{fcc} + 2/3\,{}^0G_{Sr}^{fcc} - 56196.2 + 1.90T$
	Exponential model	$G_{Pb:Sr}^{Sr_2Pb} = 1/3\,{}^0G_{Pb}^{fcc} + 2/3\,{}^0G_{Sr}^{fcc} - 52113.4 + 4.40\mathrm{T}$

[a] All parameters are given in J/mole and temperature (T) in K. The Gibbs energies for the pure elements are from the SGTE compilation [26].

The calculated Pb–Sr phase diagram using the present two sets of thermodynamic parameters are shown in Fig. 1 and Fig. 2 together with the invariant reaction temperatures and experimental data. Fig. 1 (a) presents the calculated phase diagram using the linear equation, while Fig. 1 (b) displays the calculated Pb-rich part of the phase diagram. Fig. 2 (a) is the computed phase diagram based on the exponential model and Fig. 2 (b) is the Pb-rich part of the diagram. The calculated temperatures of three eutectic points using linear model are 324.7 °C at 0.86 at.% Sr, 628.4 °C at 30.94 at.% Sr and 725.6 °C at 95.53 at.% Sr, respectively. And the calculated temperatures using exponential model are 325.9 °C at 0.65 at.% Sr, 631.0 °C at 31.13 at.% Sr and 724.0 °C at 94.95 at.% Sr, respectively. It is noted that small discrepancies exist between the calculated results using linear and exponential models. The optimized results agree well with the experimental data [6–8] except for the composition of the eutectic point (L ↔ Sr_2Pb + (Sr)ht).

Comparisons between the experimental and calculated invariant equilibria are listed in Table 4.

Table 4. *Calculated invariant equilibria in the Pb–Sr system along with the experimental data.*

Reaction	Type	T, (°C)	at.% Sr	Source
L ↔ (Pb) + $SrPb_3$	Experiment	327	~1.3	[5]
		327 ± 5	–	[6]
		324.5 ± 0.4	~1.0	[7]
		327	–	[8]
	Calculation, R-K linear model	324.7	0.86	This work
	Calculation, exponential model	325.9	0.65	This work
L ↔ $SrPb_3$	Experiment	665	25	[5]
		675	25	[6]
		677	25	[7]
		676	25	[8]
	Calculation, R-K linear model	673.1	25	This work
	Calculation, exponential model	673	25	This work
L ↔ $SrPb_3$ + Sr_3Pb_5	Experiment	627	30.6	[6]
		629 ± 3	~36	[7]
	Calculation, R-K linear model	628.4	30.94	This work
	Calculation, exponential model	631	31.13	This work
L + Sr_2Pb_3 ↔ Sr_3Pb_5	Experiment	645	~31.7	[6]
	Calculation, R-K linear model	647.4	32.38	This work
	Calculation, exponential model	644.3	32.12	This work

Table 4 is continued on the next page.

Table 4 continues from the previous page

L + SrPb ↔ Sr_2Pb_3	Experiment	717	39.9	[6]
	Calculation, R-K linear model	712.3	39	This work
	Calculation, exponential model	715.6	39.78	This work
L + Sr_5Pb_4 ↔ SrPb	Experiment	785	44.4	[6]
	Calculation, R-K linear model	787.3	42.61	This work
	Calculation, exponential model	785.1	43.16	This work
L + Sr_5Pb_3 ↔ Sr_5Pb_4	Experiment	943	53	[6]
	Calculation, R-K linear model	942.4	50.7	This work
	Calculation, exponential model	943	51.22	This work
L + Sr_2Pb ↔ Sr_5Pb_3	Experiment	1054	62.1	[6]
	Calculation, R-K linear model	1053.7	56.69	This work
	Calculation, exponential model	1054.1	56.94	This work
L ↔ Sr_2Pb	Experiment	970	70.3	[5]
		1155	66.67	[6]
	Calculation, R-K linear model	1154.2	66.67	This work
	Calculation, exponential model	1155	66.67	This work
L ↔ Sr_2Pb + (Sr)ht	Experiment	630	85.88	[5]
		725	88.4	[6]
	Calculation, R-K linear model	725.6	95.53	This wok
	Calculation, exponential model	724	94.95	This work

Except for the experimental data reported by Vakhobov et al. [5], the other experimental invariant equilibria are well reproduced by this assessment.

Fig. 3 is the calculated enthalpies of formation for the intermetallic compounds at 298.15 K based on both the linear (red solid line) and exponential (dashed line) models with the results of first-principles by Duan et al. [24] and Peng et al. [25]. The enthalpies of formation for the intermetallic compounds ($SrPb_3$, Sr_2Pb_3, SrPb, Sr_5Pb_4, Sr_5Pb_3 and Sr_2Pb) are also calculated in the present work via first-principles technique. The first-principles calculation is not performed for the Sr_3Pb_5 since its crystal structure is not well established.

The present first-principles calculation is based on density functional theory (DFT) [31, 32], which is implemented in the Vienna Ab-initio Simulation Package (VASP). The interaction between ions and electrons by using the projector augmented wave (PAW) method [33]. The exchange and correlation items are described by generalized gradient approximation (GGA) [34] refined by Perdew, Burke and Ernzerhof (PBE). The cutoff energy for plane waves was selected as 250 eV after convergence in this work. The *k* points in the first irreducible Brillouin zone were 6 × 6 × 6, 4 × 4 × 6, 6 × 2 × 6, 4 × 2 × 4, 6 × 6 × 4, 4 × 6 × 2 for $SrPb_3$, Sr_2Pb_3, SrPb, Sr_5Pb_4, Sr_5Pb_3 and Sr_2Pb, respectively. The computed enthalpies of formation presently are –33.758 kJ/(mol·atom) for $SrPb_3$, –42.806 kJ/(mol·atom) for Sr_2Pb_3, kJ/(mol·atom) for SrPb, –48.353 kJ/(mol·atom) for Sr_5Pb_4, –49.976 kJ/(mol·atom) for Sr_5Pb_3 and –50.847 kJ/(mol·atom) for Sr_2Pb, respectively.

The differences among the present first-principles calculation and those from both Duan et al. [24] and Peng et al. [25] would be probably attributed to the different theoretical methods. Duan et al. [24] and Peng et al. [25] performed the calculations by means of CASTEP (Cambridge sequential total energy package) package [35] based on DFT [31, 32]. The core-valence interactions were described by ultra-soft pseudo-potentials. Duan et al. [24] used GGA [34] function to describe the exchange correlation energy and

Peng et al. [25] used the local density approximation (LDA) CA-PZ function [36, 37]. The calculated enthalpies of formation according to the present CALPHAD modeling are a good compromise among these first-principles calculation values, as shown in Fig. 3.

Fig. 4 shows the calculated enthalpy of mixing in the liquid phase at 1200 °C by using the linear and exponential parameters, respectively. Although there are no experimental data, the interaction parameters for liquid are reasonable in view of its compatible magnitude with the computed enthalpies of formation for the solid solution phases, as shown in Fig. 3.

The present work demonstrates that both the R-K linear equation and exponential equation for the excess Gibbs energy of liquid can describe the properties of liquid phase satisfactory. In comparison with the linear equation, the unique feature of the exponential equation is that no constraint is imposed during the thermodynamic optimization in order to avoid the possible formation of undesired miscibility gap in the liquid phase. Thus the exponential equation is preferable for the future thermodynamic modeling.

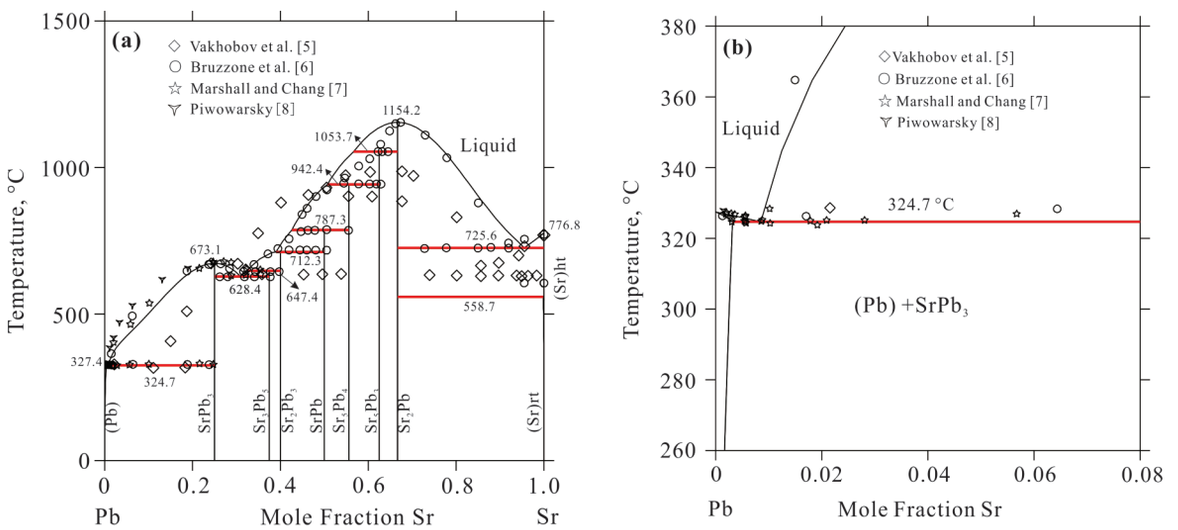

Figure 1. ***(a)*** *Calculated Pb–Sr phase diagram with linear parameters, compared with the experimental data [5–8] in the whole composition range;* ***(b)*** *The Pb-rich part of Pb–Sr phase diagram in comparison with the experimental data [5–8] from Pb to 8 at.% Sr.*

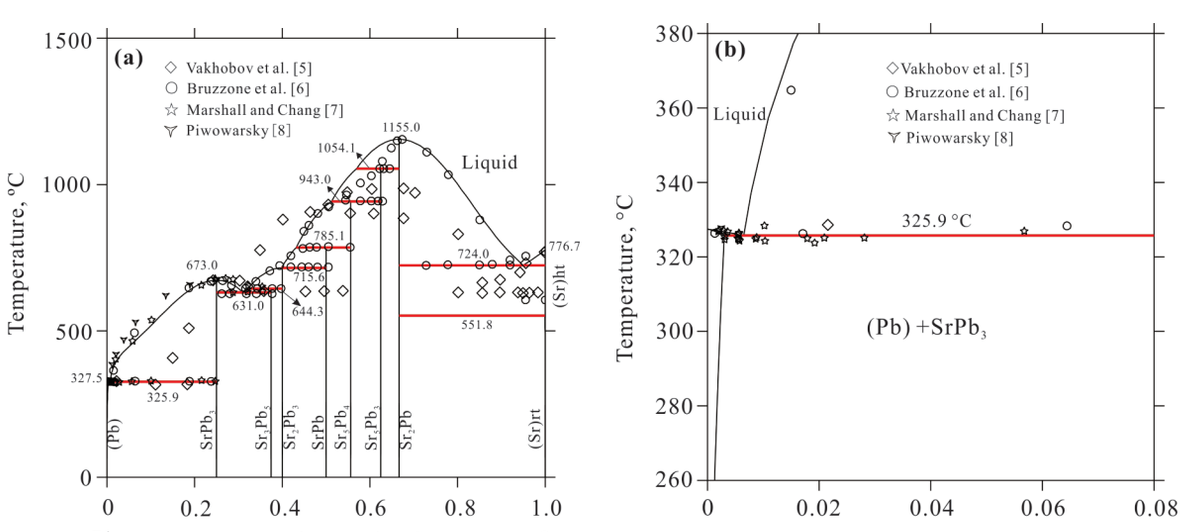

Figure 2. ***(a)*** *Calculated Pb–Sr phase diagram with exponential parameters, compared with the experimental data [5–8] in the whole composition range;* ***(b)*** *The Pb-rich part of Pb–Sr phase diagram in comparison with the experimental data [5–8] from Pb to 8 at.% Sr.*

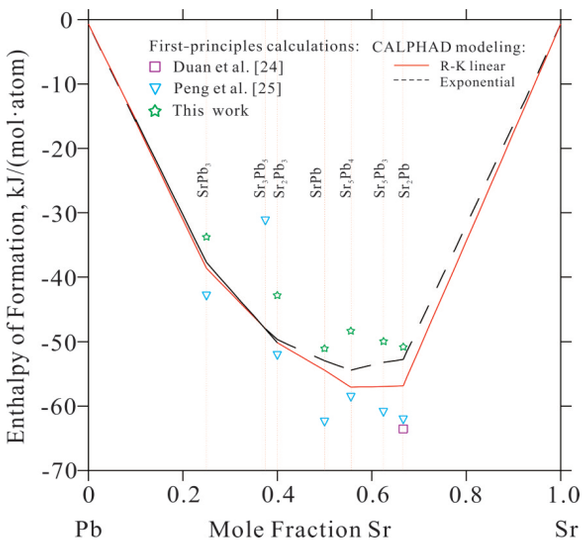

Figure 3. *Calculated enthalpies of formation for stoichiometric compounds at 298.15 K using two kinds of models in the Pb–Sr system together with previous first-principles calculations [24, 25] and present calculations.*

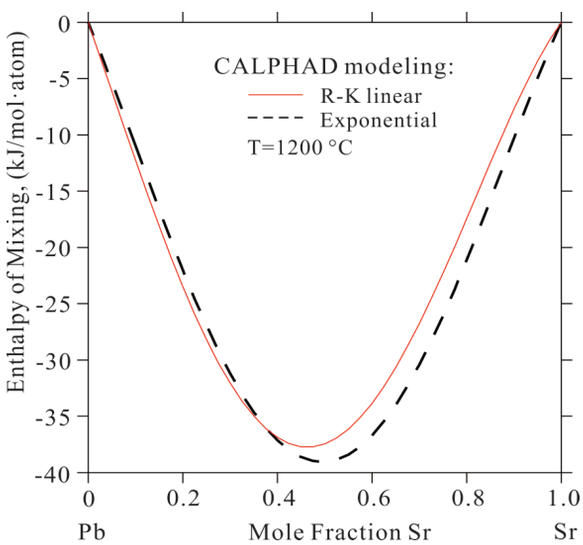

Figure 4. *Calculated enthalpies of mixing for the liquid using two kinds of parameters at 1200 °C.*

5. Conclusions

The phase diagram and thermodynamic data available for the Pb–Sr system have been critically evaluated. The enthalpies of formation for the six intermetallic compounds have been calculated by means of the first-principles calculations. On the basis of reliable phase diagram data and the first-principles computed enthalpies of formation values, two optimal sets of thermodynamic functions for the system were obtained by using both Redlich-Kister linear and exponential formulations. The comprehensive comparisons show that the experimental phase diagram data and thermodynamic data are reasonably accounted for by the present description of the Pb–Sr system.

Acknowledgment

The financial support from the National Science Foundation of China (Grant no. 51531009) is greatly acknowledged.

References

[1] J.L. Caillerie, L. Albert, J. Power Sources, 67 (1997) 279–281.
[2] D. Slavkov, B.S. Haran, B.N. Popov, F. Fleming, J. Power Sources, 112 (2002) 199–208.
[3] N.E. Bagshaw, J. Power Sources, 2 (1978) 337–350.
[4] H. Wen, F. Sheng, J. Power Sources, 33 (1991) 21–26.
[5] A.V. Vakhobov, T.D. Dzhurayev, V.A. Bardin, G.A. Zademidko, Izv. Akad. Nauk SSSR, Met., 1 (1975) 194–197 (in Russian).
[6] G. Bruzzone, E. Franceschi, F. Merlo, J. Less-Common Met., 81 (1981) 155–160.
[7] D. Marshall, Y.A. Chang, Metall. Trans. A, 15A (1984) 43–54.
[8] E. Piwowarsky, Z. Metallkunde, 14 (1922) 300–301.
[9] T.B. Massalski, (editor-in-chief): "Binary Alloy Phase Diagrams", Second Edition, Vol. 3, T.B. Massalski (editor-in-chief), Materials Information Soc., Materials Park, Ohio (1990).
[10] J. Zhao, J. Zhou, S. Liu, Y. Du, S. Tang, Y. Yang, J. Min. Metall. Sect. B-Metall., 52 (1) B (2016) 99–112.
[11] G. Huang, L. Liu, L. Zhang, Z. Jin, J. Min. Metall. Sect. B-Metall., 52 (2) B (2016) 177–183.
[12] B. Hu, B. Yao, J. Wang, J.-R. Zhao, F.-F. Min, Y. Du, J. Min. Metall. Sect. B-Metall., 53 (2) B (2017) 95–106.
[13] O. Redlich, A. Kister, Ind. Eng. Chem., 40 (1948) 345–348.
[14] G. Kaptay, CALPHAD 28 (2004) 115–124.
[15] G. Bruzzone, E.A. Franceschi, J. Less-Common Met., 57 (1978) 201–208.
[16] G. Bruzzone, E.A. Franceschi, F. Merlo, J. Less-Common Met., 60 (1978) 59–63.
[17] F. Merlo, M.L Fornasini, J. Less-Common Met., 13 (1967) 603–610.
[18] F. Merlo, Rev. Chim. Miner., 21 (1984) 78–84.
[19] E. Zintl, S. Neumar (in German), Z. Elektrochem., 39 (1933) 86–97.
[20] H. Damsma, E.E. Havinga, J. Phys. Chem. Solids, 34 (1973) 813–816.
[21] J.J. Van Der Brook, Scr. Metall., 6 (1972) 311–315.
[22] G. Bruzzone, J. Less-Common Met., 11 (1966) 249–258.
[23] E.A. Sheldon, A.J. King, Acta Crystallogr., 6 (1953) 100.
[24] Y.H. Duan, W.C. Hu, Y. Sun, M.J. Peng, J. Alloys Compd. 614 (2014) 334–344.
[25] M.J. Peng, Y.H. Duan, Y. Sun, Comput. Mater. Sci., 98

(2015) 311–319.
[26] A.T. Dinsdale, CALPHAD, 15 (4) (1991) 417–425.
[27] B. Sundman, B. Janson, J.O. Andersson, CALPHAD, 9 (1985) 153–190.
[28] Y. Du, R. Schmid-Fetzer, H. Ohtani, Z. Met., 88 (1997) 545–556.
[29] C.H. Lupis, Chemical Thermodynamics of Metals, Prentice-Hall Inc., North-Holland, NY, 1983.
[30] K.C. Kumar, P. Wollants, J. Alloys Compd., 320 (2001) 189–198.
[31] P. Hohenberg, W. Kohn, Phys. Rev., 136 (1964) B864–B871.
[32] W. Kohn, L.J. Sham, Phys. Rev., 140 (1965) A1133–A1138.
[33] G. Kresse, D. Joubert, Phys. Rev. B, 59 (1999) 1758–1775.
[34] J.P. Perdew, K. Burke, M. Ernzerhof, Phys. Rev. Lett., 77 (1996) 3865–3868.
[35] M.D. Segall, P.J.D. Lindan, M.J. Probert, C.J. Pickard, P.J. Hasnip, S.J. Clark, M.C. Payne, J. Phys.: Condens. Matter. 14 (2002) 2717–2744.
[36] D.M. Ceperley, B.J. Alder, Phys. Rev. Lett. 45 (1980) 566–579.
[37] J.P. Perdew, A. Zunger, Phys. Rev. B 23 (1981) 5048–5079.